Journal of Power Sources 195 (2010) 4384–4390

Contents lists available at ScienceDirect

Journal of Power Sources

journal homepage: www.elsevier.com/locate/jpowsour

Low molecular mass organogelator based gel electrolyte gelated by a quaternary ammonium halide salt for quasi-solid-state dye-sensitized solar cells

Zhipeng Huo[a,b], Changneng Zhang[a,b], Xiaqin Fang[a,b], Molang Cai[a,b], Songyuan Dai[a,b,*], Kongjia Wang[a,b]

[a] Key Lab of Novel Thin Film Solar Cells, Chinese Academy of Sciences, PR China
[b] Institute of Plasma Physics, Chinese Academy of Sciences, PR China

ARTICLE INFO

Article history:
Received 30 September 2009
Received in revised form
10 December 2009
Accepted 17 December 2009
Available online 14 January 2010

Keywords:
Low molecular mass organogelator
Tetradodecylammonium bromide
Electron recombination
Stability
Quasi-solid-state
Dye-sensitized solar cell

ABSTRACT

Quasi-solid-state dye-sensitized solar cells (DSC) are fabricated using tetradodecylammonium bromide as a low molecular mass organogelator (LMOG) to form gel electrolyte with a high solution-to-gel transition temperature (T_{SG}) of 75 °C to hinder flow and volatilization of the liquid. The steady-state voltammograms reveal that the diffusion of the I_3^- and I^- in the gel electrolyte is hindered by the self-assembled network of the gel. An increased interfacial exchange current density (j_0) of 4.95×10^{-8} A cm^{-2} and a decreased electron recombination lifetime (τ) of 117 ms reveal an increased electron recombination at the dyed TiO_2 photoelectrode/electrolyte interface in the DSC after gelation. The results of the accelerated aging tests show that the gel electrolyte based dye-sensitized solar cell can retain over 93% of its initial photoelectric conversion efficiency value after successive heating at 60 °C for 1000 h, and device degradation is negligible after one sun light soaking with UV cutoff filter for 1000 h.

1. Introduction

Dye-sensitized solar cells (DSC) which are most attractive candidates due to their low production cost in comparison to conventional inorganic photovoltaic devices are currently attracting widely to both academic and commercial interests [1]. An impressive photoelectric conversion efficiency greater than 10% has been obtained for photovoltaic devices with organic solvent based electrolytes [2–8], and our 500 W DSC showcase for outdoor application was founded in 2004, which gives a picture of the prospective industrial application in the near future [9]. However, the presence of liquid electrolytes in such modules may result in some practical limitations of sealing and long-term stability caused by the leakage of the liquid electrolyte. Therefore, p-type semiconductor [10,11], hole-conductor [12], and polymeric materials incorporating the redox couple I_3^-/I^- [13–17], which can be used as solid-state electrolyte, have been attempted to substitute for the liquid electrolyte in DSC. However, the contact between hole transporting materials and the nanoporous semiconductor films is under development, and the photovoltaic performance of solid-state DSC is still too low for practical application.

According to the reports, gelation of organic solvent based or ionic liquid based liquid electrolytes with polymers [18–20], nanoparticles [21–23], or low molecular mass organogelators (LMOGs) [24,25] can produce quasi-solid-state electrolytes for dye-sensitized solar cells with good photovoltaic performance. The low molecular mass organogelators constitute an important class of functional materials with a broad range of applications in templated material synthesis, drug delivery systems, personal care products, separation technology, and biomimetics [26–31]. The molecules of LMOGs are capable of self-organizing into finely dispersed anisotropic aggregates within the organic solvent to form three-dimensional (3D) structure by very specific and balanced supramolecular interactions of the gelator molecules such as hydrogen bonding, hydrophobic interactions, π–π interactions, and electrostatic interactions [24]. Such network structures commonly melt upon heating but are reformed again during the cooling process, revealing the thermoreversibility of the system. This is an advantage of the LMOGs. Because of the thermoreversibility, above the solution-to-gel transition temperature (T_{SG}), the hot solution of the electrolyte can efficiently fill the nanopores of the nanoporous TiO_2 photoelectrode, and upon cooling, the molecules of LMOGs are self-assembling to form a 3D network in the internal space between the nanoporous TiO_2 photoelectrode and the counter electrode of

* Corresponding author at: Key Lab of Novel Thin Film Solar Cells, Institute of Plasma Physics, Chinese Academy of Sciences, P.O. Box 1126, Hefei, Anhui, 230031, PR China. Tel.: +86 551 5591377; fax: +86 551 5591377.
E-mail address: sydai@ipp.ac.cn (S. Dai).

0378-7753/$ – see front matter © 2010 Elsevier B.V. All rights reserved.
doi:10.1016/j.jpowsour.2009.12.107

Fig. 1. Photo of liquid and low molecular mass organogelator based gel (the bottle is upside down) electrolytes (from left to right).

the DSC; then, a mechanically stable quasi-solid-state electrolyte is obtained. These characteristics triggered our interest to develop LMOG based gel electrolytes for quasi-solid-state dye-sensitized solar cells.

Recently, research on applying LMOG based gel electrolytes to quasi-solid-state DSC, and the long-term stability of the LMOG based DSC is still very few. According to the reports, small concentrations of some structurally simple tertiary amines and related tertiary and quaternary ammonium halide salts form viscoelastic, thermally reversible gels with organic liquids [32]. In this paper, for the first time, tetradodecylammonium bromide was introduced into 3-methoxypropionitrile (MePN) based liquid electrolyte as a low molecular mass organogelator to form gel electrolyte for quasi-solid-state dye-sensitized solar cells (shown in Fig. 1). We report our research results about the gelation ability of this kind of LMOG, the influence on the charge transportation in the electrolyte, the charge recombination at the dyed TiO_2 photoelectrode/electrolyte interface, the photovoltaic performance, and both the thermostability and photostability of the corresponding quasi-solid-state dye-sensitized solar cells in detail.

2. Experimental

2.1. Preparation of dye-sensitized nanoporous TiO_2 photoelectrode

By screen-printing double layer 25-nm-sized TiO_2 nanoparticles [33] on transport conducting glass (FTO, TEC-8, LOF), a 20 μm thick TiO_2 film was prepared as photoelectrode; then, it was coated with a 3 μm thick 300 nm-sized light-scattering anatase particles. After sintering at 500 °C for 30 min in air then cooling to about 80 °C, the nanoporous TiO_2 photoelectrode was immersed in an anhydrous ethanol solution with 5×10^{-4} mol L^{-1} *cis*-dithiocyanate-*N*,*N*′-bis-(4-carboxylate-4-tetrabutylammonium carboxylate-2,2′-bipyridine) ruthenium(II) (N719) for 12 h and then assembled with platinized counter electrode. Two electrodes were separated by hot-melt Surlyn polymer film and sealed up by heating.

2.2. Preparation of the electrolytes

1,2-Dimethyl-3-propylimidazolium iodide (DMPII) was synthesized as reported previously [34]. The composition of liquid electrolyte A is as follows: 0.6 mol L^{-1} 1,2-dimethyl-3-propylimidazolium iodide, 0.1 mol L^{-1} lithium iodide anhydrous (98%, Fluka), 0.1 mol L^{-1} iodine, 0.45 mol L^{-1} *N*-methylbenzimidazole (NMBI: 99%, Aldrich) in 3-methoxypropionitrile (MePN: 99%, Fluka). The gel electrolyte B was prepared by adding 10 wt% (*vs.* liquid electrolyte A) tetradodecylammonium bromide (99%, Fluka) into liquid electrolyte A and heated under stirring until the low molecular mass organogelator melted. After cooling down to room temperature, the gel electrolyte was formed.

2.3. Fabrication of the DSC

By using a vacuum pump, the liquid electrolyte was injected into the internal space of the cell through the hole on the counter electrode, and the hole was sealed by heating the hot-melt Surlyn film between the thin glass cover and counter electrode. The gel electrolyte was heated to 90 °C under stirring until the gel completely melted. Then, the electrolyte (hot solution) was injected into the internal space of the cell through the hole made on the counter electrode, and the hole was sealed by heating the hot-melt Surlyn film between the thin glass cover and counter electrode. After cooling down to room temperature, a uniform motionless gel layer was formed in cell.

2.4. Differential scanning calorimetry

The solution-to-gel transition temperature (T_{SG}) of the gel electrolyte was determined by using differential scanning calorimeter (DSC821^e/700 METTLER TOLEDO). The measurements were performed with samples of 10–30 mg at a heating rate of 5 °C min^{-1} under nitrogen in a temperature range of 10–110 °C.

2.5. Voltammetric measurements

Steady-state voltammetry was adopted in a conventional photoelectrochemical cell equipped with a 5.0 μm platinum ultramicroelectrode (CHI107) as working electrode, and with a 1 mm radius platinum disk electrode (CHI102) as counter electrode and reference electrode. A slow scan rate of 5 mV s^{-1} was used in order to obtain steady-state current–voltage curves. This work was carried out at 25 °C on an electrochemical workstation (CHI660A, CH Instruments Inc., Austin, TX). The dark current–voltage characteristic data were obtained by linear sweep voltammetry by using an electrochemical workstation (CHI660A, CH Instruments Inc., Austin, TX). The working electrode was the dye-sensitized TiO_2 film of DSC. The auxiliary electrode and the reference electrode were the platinized conducting glass of DSC. The scan rate was 10 mV s^{-1}.

2.6. Electrochemical impedance measurements

Impedance measurements were performed with a computer-controlled potentiostat (IM6ex, Zahner, Germany) in the frequency range from 20 mHz to 1000 kHz. The magnitude of the alternative signal was 5 mV. The impedance measurements were carried out in dark and the obtained spectra were fitted with Z-View software in terms of appropriate equivalent circuits.

2.7. Tafel polarization measurements

Tafel plots were recorded on an electrochemical workstation (CHI660A, CH Instruments Inc., Austin, TX) at room temperature in two-electrode mode of DSC as reported previously [35]. The

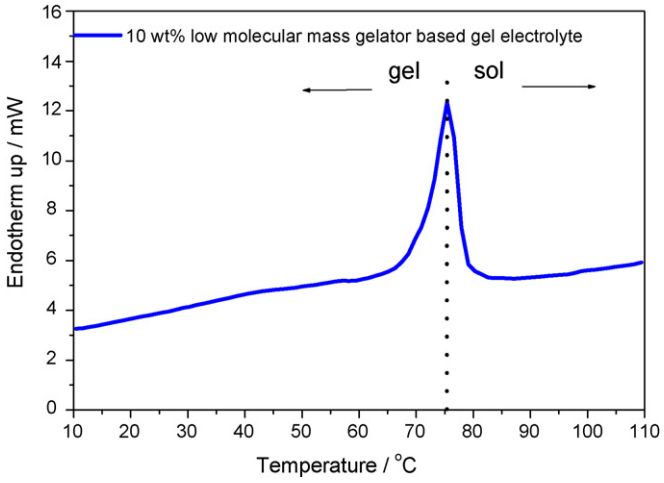

Fig. 2. Differential scanning calorimetric thermograms of the low molecular mass organogelator based gel.

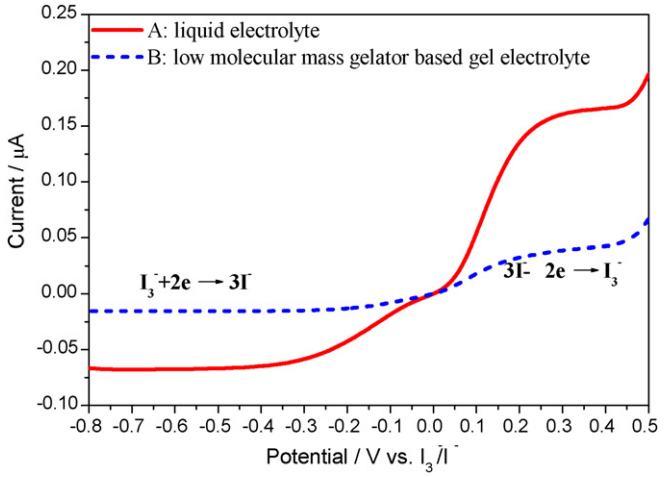

Fig. 3. Steady-state voltammograms of the liquid (A) and gel electrolyte (B) with Pt ultramicroelectrode at the scan rate of 5 mV s^{-1} at 25 °C.

scan rate was 0.2 mV s^{-1}. The exchange current density (j_0) was evaluated from the intersection of the linear anodic and cathodic branches of the polarization curves.

2.8. Photoelectrochemical measurements

The photovoltaic performance of DSC was measured by a Keithley 2420 source meter controlled by Testpoint software under solar simulator (Xenon lamp, AM 1.5, 100 mW cm^{-2}, Changchun Institute of Optics Fine Mechanics and Physics, Chinese Academy of Sciences, calibrated with standard crystalline silicon solar cell). The incident light intensity was calibrated with a standard crystalline silicon solar cell before each experiment. The total covered active electrode area with black mask of DSC was 0.16 cm^2. Hermetically sealed cells were used for long-term stability tests. The cells were stored in the oven at 60 °C for thermal stress. During successive one sun light soaking experiment, the cells covered with UV cut-off filter (up to 394 nm) were irradiated at open circuit under a Xenon lamp (XQ3000, 100 mW cm^{-2}, Shanghai DianGuang Equipment Ltd., China) and the air temperature was set to approximately 50 °C.

3. Results and discussions

3.1. Gelation studies of the low molecular mass organogelator based gel

The thermogram of the gel shows an endothermic signal with its maximum at 75 °C (shown in Fig. 2) corresponding to the solution-to-gel transition temperature (T_{SG}). This high transition temperature means that below 75 °C the electrolyte maintains a gel state and above this point the network collapses and a liquid is obtained. The gelation of the liquid hinders flow of the liquid, and this high T_{SG} ensure the gel state of the electrolyte at operating temperature of the solar cell.

3.2. Electrochemical characteristics of the gel electrolyte

We characterized the electrochemical properties of the gel electrolyte in detail. Fig. 3 is the comparative steady-state voltammograms for the liquid electrolyte and gel electrolyte at 25 °C. The apparent diffusion coefficient (D_{app}) values of iodide and triiodide (shown in Table 1) were calculated from the anodic and cathodic steady-state current (I_{ss}) using the following equation [36].

$$I_{ss} = 4naCFD_{app} \quad (1)$$

where n is the electron number in the electrode reaction, F is the Faraday constant, and C is the bulk concentration of electroactive species, D_{app} is the apparent diffusion coefficient, a is the radius of the Pt ultramicroelectrode. From the apparent diffusion coefficient data shown in Table 1, it can be obviously seen that the apparent diffusion coefficients of iodide and triiodide changes remarkably after gelation. The apparent diffusion coefficients of iodide and triiodide in the liquid electrolytes (electrolyte A) are several times lager than that in the gel electrolyte (electrolyte B). The apparent diffusion coefficient of I_3^- decreased from 4.16×10^{-10} m^2 s^{-1} to 1.01×10^{-10} m^2 s^{-1}, and the apparent diffusion coefficient of I^- decreased from 8.74×10^{-11} m^2 s^{-1} to 2.02×10^{-11} m^2 s^{-1}. These results suggested that the channel for the charge transport in gel electrolyte was altered by the self-assembled network constructed by the low molecular mass organogelator [37]. Therefore, the network of this kind of gel hindered the diffusion of the charges in the electrolyte.

3.3. Studies of the charge recombination at the dyed TiO_2 photoelectrode/electrolyte interface

Tafel analysis was used to study the interfacial charge-transfer properties of the I^-/I_3^- redox on the TiO_2 surface [35]. At the photoelectrode in DSC, the rates of cathodic and anodic reactions at the semiconductor/electrolyte interface can be described by the Butler–Volmer equation [38,39].

$$j = -j_0 \left[\exp \frac{\alpha_c nF}{RT}(E - E_{eq}) - \exp \frac{-\alpha_a nF}{RT}(E - E_{eq}) \right] \quad (2)$$

where j is the total current density, j_0 is the exchange current density, E is the applied voltage, E_{eq} is the I^-/I_3^- electrode potential at equilibrium, n is the number of electrons transferred, α is the

Table 1
The steady-state current and apparent diffusion coefficient of iodide and triiodide in different electrolytes.[a]

Electrolyte	$10^8 I_{ss}$ (A)		$10^{11} D_{app}$ (m^2 s^{-1})	
	I_3^-	I^-	I_3^-	I^-
Liquid electrolyte (A)	16.1	6.75	41.6	8.74
Gel electrolyte (B)	3.88	1.56	10.1	2.02

[a] Measured at 25 °C.

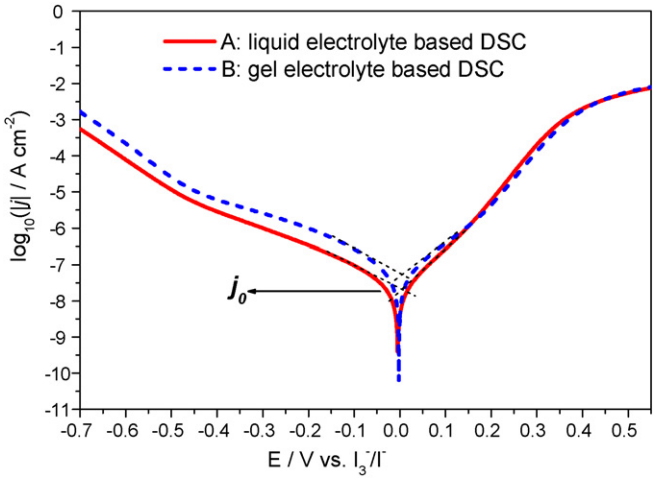

Fig. 4. Tafel curves of dye-sensitized solar cells based on the liquid electrolyte (A) and gel electrolyte (B) in the dark. The scan rate was 0.2 mV s^{-1}.

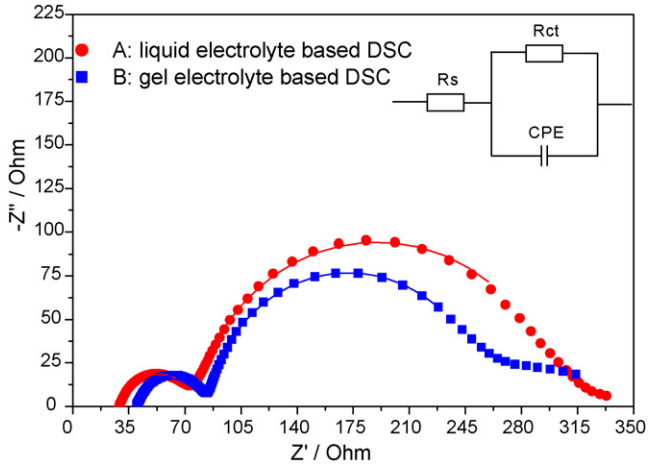

Fig. 5. Nyquist plots of the liquid electrolyte based cell (A) and gel electrolyte based cell (B) measured at −0.65 V in the dark. The lines show the fitted results. Equivalent circuit used for the curve fitting of the impedance spectra is shown in the inset.

transfer coefficient, and a and c are the anodic and cathodic transfer coefficient, respectively. In Eq. (2), the first term on the right side is proportional to the cathodic current, and the second term is proportional to the anodic current. It is clear that $j = j_0$ when $E = E_{eq}$ in the dark, and j_0 depends on the reaction area and the concentrations of I^-/I_3^- on the photoelectrode. The exchange current density (j_0) was calculated the intersection of the linear anodic and cathodic branches of the polarization curves.

$$\beta = 2.303\frac{RT}{\alpha F} \quad (3)$$

The Tafel slope, β (Eq. (3)), is proportional to $1/\alpha$. The linear regions of the polarization profiles have slopes equal to β_a and β_c and are known as the anodic and cathodic Tafel regions. The β_a and β_c values are indicative of the anodic and cathodic reactions occurring on the TiO_2/electrolyte interface.

Fig. 4 shows Tafel polarization experiments to gain insight into the electrode kinetics for DSC based on the liquid electrolyte and gel electrolyte. After gelation, the exchange current density for the I^-/I_3^- couple at the TiO_2/electrolyte interface was about 4.95×10^{-8} A cm^{-2}. This was much higher than that of the DSC based on the liquid electrolyte (i.e., 1.98×10^{-8} A cm^{-2}). The gelation caused an increase in the exchange current density to decrease the charge transfer resistance at the photoelectrode/electrolyte interface.

Lower cathodic Tafel slope (β_c) value was found in the gel electrolyte based DSC as shown in Fig. 4 and Table 2. The gel electrolyte based DSC exhibited a cathodic Tafel slope value close to 146 mV decade^{-1}, which corresponds to the recombination reaction at the dyed TiO_2 photoelectrode/electrolyte interface between electrons from the conduction band of TiO_2 and I_3^- in the electrolyte. The decreased cathodic Tafel slope indicated that the gelation of the electrolyte had increased the reaction of the I_3^- ions at the dyed TiO_2 photoelectrode/electrolyte interface. A higher anodic Tafel slope (β_a) value was found in the gel electrolyte based DSC, denoting a decreased reaction of I^- ions at the dyed TiO_2 photoelectrode/electrolyte interface.

In the dark, the DSC behaves as a leaking capacitor [40]. Under forward bias in the dark, electrons are transported through the nanoporous TiO_2 photoelectrode and react with I_3^-. At the same time, I^- is oxidized to I_3^- at the counter electrode. The dark reaction impedance caused by electron transfer from the conduction band of the nanoporous TiO_2 film to triiodide ions in the electrolyte is presented by the semicircle in intermediate frequency regime in the Nyquist plots [41]. The bigger the middle frequency semicircle in the Nyquist plots is, the slighter the electron recombination at the dyed TiO_2 photoelectrode/electrolyte interface is. Fig. 5 shows the Nyquist plots of the liquid electrolyte based cell (electrolyte A) and gel electrolyte based cell (electrolyte B) measured at −0.65 V bias in dark. Fitting the middle frequency semicircle gives the chemical capacitance (C_μ) and the electron transport resistance (R_{ct}). The fitting results are presented in Table 3, after gelation by this kind of low molecular mass organogelator, C_μ increased from 2437 to 2703 μF cm^{-2}, while R_{ct} reduced from 241 Ω to 174 Ω, yielding a shorter electron recombination lifetime (τ) of 117 ms for the gel electrolyte based cell than that for the liquid electrolyte based cell (i.e., 147 ms). The decrease of τ by gelating the electrolyte revealed a more rapid decrease of the conduction band of the semiconductor than that of the liquid electrolyte based device and an increase of the electron recombination at the dyed TiO_2 photoelectrode/electrolyte interface, which was caused by the conduction band electrons of nanoporous TiO_2 photoelectrode captured by the reduction of I_3^- ions.

Fig. 6 shows the dark current–voltage characteristics of the liquid electrolyte and low molecular mass organogelator based gel electrolyte. The dark current–voltage characteristic experiments were performed to investigate the charge recombination at the dyed TiO_2 photoelectrode/electrolyte interface. The results revealed that, after gelation, the dark reaction at the dyed TiO_2 photoelectrode/electrolyte interface was increased.

Table 2
The results derived from the Tafel polarization curves in Fig. 4 for the dye-sensitized solar cells in the dark.

	Liquid electrolyte (A)	Gel electrolyte (B)
j_0 (nA cm^{-2})	19.8	49.5
β_c (mV decade^{-1})	159	146
β_a (mV decade^{-1})	83	106

Table 3
The fitting results of EIS parameters for the DSC of cell A and cell B measured under −0.65 V in the dark.[a]

Cell	R_{ct} (Ω)	C_μ (μF cm^{-2})	τ (ms)
A	241	2437	147
B	174	2703	117

[a] Cell A is DSC with the liquid electrolyte, and cell B is DSC with the gel electrolyte.

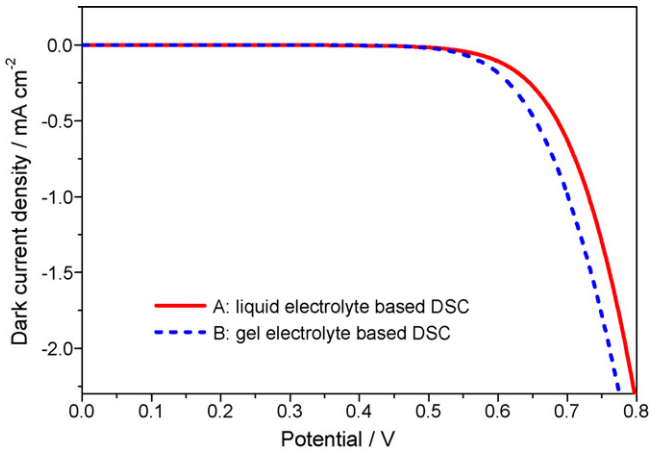

Fig. 6. Dark current–voltage characteristics of the liquid electrolyte based cell (A) and gel electrolyte based cell (B) at the scan rate of 10 mV s^{-1}.

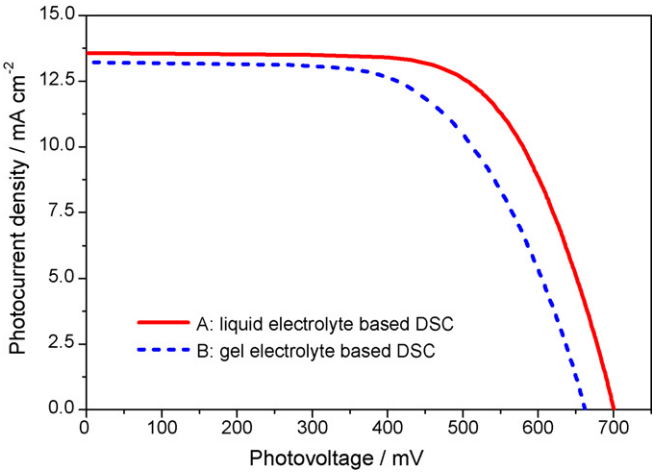

Fig. 7. Photocurrent density–voltage characteristics of DSC based on the liquid electrolyte (A) and low molecular mass organogelator based gel electrolyte (B) at AM 1.5.

3.4. Photovoltaic performance of quasi-solid-state dye-sensitized solar cell fabricated using low molecular mass organogelator

Fig. 7 shows the photocurrent density–voltage characteristics of liquid electrolyte and gel electrolyte based devices at AM 1.5 (one sun). Table 4 summarizes the photovoltaic performance parameters of dye-sensitized solar cells based on liquid electrolyte and low molecular mass organogelator based gel electrolyte at an irradiation of AM 1.5. These data show that the device based on the low molecular mass organogelator based gel electrolyte (cell B) got a slightly lower photovoltaic performance than the device based on the corresponding liquid electrolyte (cell A). It had smaller short-circuit current density (J_{sc}), open circuit voltage (V_{oc}), fill factor (*FF*), and photoelectric conversion efficiency (η) than that based on the corresponding liquid electrolyte.

Table 4
Photovoltaic performance parameters of dye-sensitized solar cells based on liquid electrolyte and low molecular mass organogelator based gel electrolyte.[a]

Cell	J_{sc} (mA cm^{-2})	V_{oc} (V)	*FF*	η
A	13.594	0.700	0.667	6.35%
B	13.219	0.662	0.611	5.35%

[a] Measured at an irradiation of AM 1.5. Cell A is DSC with the liquid electrolyte, and cell B is DSC with the gel electrolyte.

V_{oc} depends on the dark current that is related to the charge recombination between conduction band electrons and the oxidized half in the electrolyte [42]. The dark reaction is represented by Eq. (4):

$$I_3^- + 2e_{cb}(TiO_2) \xrightarrow{k_{et}} 3I^- \quad (4)$$

V_{oc} for dye-sensitized solar cells with an iodine redox electrolyte is represented by the following equation [43]:

$$V_{oc} = \frac{kT}{e}\left(\frac{I_{inj}}{n_{cb}k_{et}[I_3^-]}\right) \quad (5)$$

where k and T are the Boltzmann constant and absolute temperature, respectively, I_{inj} is the injection current from dye to semiconductor, n_{cb} is the electron density on the conduction band of semiconductor, and k_{et} represents the rate constant of reduction of I_3^- to I^-. According to Eq. (5), V_{oc} decreases with an increasing dark reaction. Decrease in V_{oc} of the gel electrolyte based devices could be explained by the enhanced dark reaction. Since the charge transport in the gel electrolyte was hindered by the self-assembled network of the gel, the transportation of I_3^- ions from the dyed TiO_2 photoelectrode/electrolyte interface to the counter electrode was slowed down. Thus, the recombination at the interface between nanoporous TiO_2 photoelectrode and the electrolyte increased; therefore, the dark current increased (shown in Fig. 6). As a result, the open circuit voltage (V_{oc}) decreased (from 0.700 to 0.662 V). Moreover, both J_{sc} and *FF* are influenced by the charge transportation of the gel electrolyte, because the decrease in charge transportation causes rate-determining of charge transportation and increasing the series resistance [44]. As a result, the short-circuit current density (J_{sc}) (from 13.594 mA cm^{-2} to 13.219 mA cm^{-2}) and fill factor (*FF*) (from 0.667 to 0.611) of the DSC decreased. Consequently, compared with the corresponding liquid electrolyte based DSC, photoelectric conversion efficiency (η) (from 6.35% to 5.35%) of the gel electrolyte based DSC decreased.

3.5. Stability of quasi-solid-state dye-sensitized solar cells fabricated using low molecular mass organogelator

Although the device based on the low molecular mass organogelator based gel electrolyte got a slightly lower photovoltaic performance than the device based on the corresponding liquid electrolyte, it exhibited good stability. In our experiment, we examined the stability of the devices based on the liquid electrolyte and the low molecular mass organogelator based gel electrolyte both under successive heating and light soaking. Fig. 8 shows the comparison of thermostability between the liquid electrolyte based device and gel electrolyte based device at 60 °C thermal stress for 1000 h.

The conversion efficiency of the gel electrolyte based device could retain over 93% of its initial value after this period. However, the conversion efficiency of the liquid electrolyte based device retained only 77% of its initial value after this period. Fig. 9 shows the comparison of stability between the liquid electrolyte based device and gel electrolyte based device during successive one sun light soaking with a UV cutoff filter for 1000 h. The conversion efficiency of the gel electrolyte based device could retain over 96% of its initial value after this period. However, the conversion efficiency of the liquid electrolyte based device retained only 87% of its initial value after this period. These results reveal that the gel electrolyte based device had better stability than the corresponding liquid electrolyte based device. This is because this gel electrolyte had excellent stability and the network of the gel hindered the leakage of the liquid electrolyte effectively.

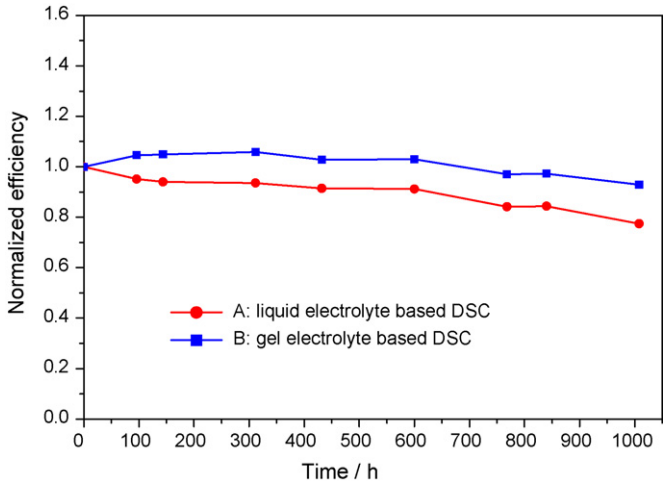

Fig. 8. Normalized device efficiency variation with the liquid electrolyte (A) and low molecular mass organogelator based gel electrolyte (B) during accelerated aging tests at 60 °C for 1000 h.

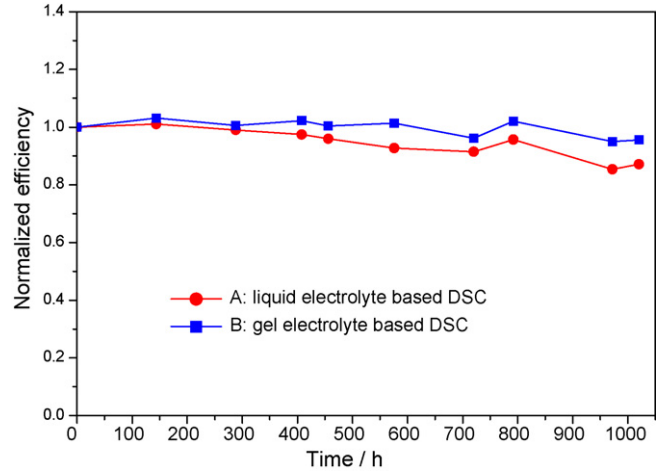

Fig. 9. Normalized device efficiency variation with the liquid electrolyte (A) and low molecular mass organogelator based gel electrolyte (B) during successive one sun light soaking with UV cutoff filter at 50 °C for 1000 h.

4. Conclusion

In summary, tetradodecylammonium bromide was successfully introduced into a MePN based liquid electrolyte as a low molecular mass organogelator to form a gel electrolyte with a high solution-to-gel transition temperature for quasi-solid-state dye-sensitized solar cells. Since the charge transport in the gel electrolyte was hindered by the self-assembled network of the gel, the transportation of I_3^- ions from the dyed TiO_2 photoelectrode/electrolyte interface to the counter electrode was slowed down. Thus, the recombination at the interface between nanoporous TiO_2 photoelectrode and the electrolyte increased; therefore, the dark current increased. As a result, the open circuit voltage (V_{oc}) decreased. Moreover, both short-circuit current density (J_{sc}) and fill factor (*FF*) of the DSC were decreased by the decrease in charge transportation of the gel electrolyte. Consequently, photoelectric conversion efficiency (η) of the gel electrolyte based DSC was lower than that of the corresponding liquid electrolyte based DSC. Importantly, although the device based on the low molecular mass organogelator based gel electrolyte got a slightly lower photovoltaic performance than the device based on the corresponding liquid electrolyte, the results of the accelerated aging tests showed that the gel electrolyte based device and liquid electrolyte based device retained 93% and 77% of their initial photoelectric conversion efficiency value respectively after heating at 60 °C for 1000 h, and the gel electrolyte based device and liquid electrolyte based device retained 96% and 87% of their initial photoelectric conversion efficiency value respectively after one sun light soaking for 1000 h, which indicates that using this kind of gel electrolyte can greatly improve the stability of DSC. These results reveal that the network of the gel hindered the leakage of the liquid electrolyte effectively, which contribute significantly to the improvement of the long-term stability of dye-sensitized solar cells. They offer us a method to realize the practical use of dye-sensitized solar cells by using a kind of low molecular mass organogelator to form a gel electrolyte for quasi-solid-state dye-sensitized solar cells with high stability and good performance, and it will enable the fabrication of flexible compact, laminated quasi-solid-state devices free of leakage and available in varied geometries.

Acknowledgments

This work was financially supported by the National Basic Research Program of China under Grant No. 2006CB202600, the National High Technology Research and Development Program of China under Grant No. 2009AA050603, and Funds of the Chinese Academy of Sciences for Key Topics in Innovation Engineering under Grant No. KGCX2-YW-326. We appreciate the cooperation of Dyesol in Australia and Prof. M. Grätzel, EPFL in Switzerland.

References

[1] M. Grätzel, Nature 414 (2001) 338–344.
[2] M.K. Nazeeruddin, A. Kay, I. Rodicio, R. Humphry-Baker, E. Müller, P. Liska, N. Vlachopoulos, M. Grätzel, J. Am. Chem. Soc. 115 (1993) 6382–6390.
[3] M.K. Nazeeruddin, P. Péchy, T. Renouard, S.M. Zakeeruddin, R. Humphry-Baker, P. Comte, P. Liska, L. Cevey, E. Costa, V. Shklover, L. Spiccia, G.B. Deacon, C.A. Bignozzi, M. Grätzel, J. Am. Chem. Soc. 123 (2001) 1613–1624.
[4] M. Grätzel, J. Photochem. Photobiol. A: Chem. 164 (2004) 3–14.
[5] Z.S. Wang, H. Kawauchi, T. Kashima, H. Arakawa, Coord. Chem. Rev. 248 (2004) 1381–1389.
[6] Z.S. Wang, M. Yanagida, K. Sayama, H. Sugihara, Chem. Mater. 18 (2006) 2912–2916.
[7] Z.S. Wang, T. Yamaguchi, H. Sugihara, H. Arakawa, Langmuir 21 (2005) 4272–4276.
[8] N. Koide, A. Islam, Y. Chiba, L.Y. Han, J. Photochem. Photobiol. A: Chem. 182 (2006) 296–305.
[9] S.Y. Dai, K.J. Wang, J. Weng, Y.F. Sui, Y. Huang, S.F. Xiao, S.H. Chen, L.H. Hu, F.T. Kong, X. Pan, C.W. Shi, L. Guo, Sol. Energy Mater. Sol. Cells 85 (2005) 447–455.
[10] C.N. Zhang, K.J. Wang, L.H. Hu, F.T. Kong, L. Guo, J. Photochem. Photobiol. A: Chem. 189 (2007) 329–333.
[11] G.R.R.A. Kumara, A. Konno, G.K.R. Senadeera, P.V.V. Jayaweera, D.B.R.A. De Silva, K. Tennakone, Sol. Energy Mater. Sol. Cells 69 (2001) 195–199.
[12] U. Bach, D. Lupo, P. Comte, J.E. Moser, F. Weissörtel, J. Salbeck, H. Spreitzer, M. Grätzel, Nature 395 (1998) 583–585.
[13] F. Cao, G. Oskam, P.C. Searson, J. Phys. Chem. 99 (1995) 17071–17073.
[14] M.A.K.L. Dissanayake, L.R.A.K. Bandara, R.S.P. Bokalawala, P.A.R.D. Jayathilaka, O.A. Ileperuma, S. Somasundaram, Mater. Res. Bull. 37 (2002) 867–874.
[15] O.A. Ileperuma, M.A.K.L. Dissanayake, S. Somasundaram, Electrochim. Acta 47 (2002) 2801–2807.
[16] P. Wang, S.M. Zakeeruddin, I. Exnar, M. Grätzel, Chem. Commun. (2002) 2972–2973.
[17] T. Asano, T. Kubo, Y. Nishikitani, J. Photochem. Photobiol. A: Chem. 164 (2004) 111–115.
[18] D. Saikia, C.C. Han, Y.W. Chen-Yang, J. Power Sources 185 (2008) 570–576.
[19] Y. Yang, C. Zhou, S. Xu, H. Hu, B. Chen, J. Zhang, S. Wu, W. Liu, X. Zhao, J. Power Sources 185 (2008) 1492–1498.
[20] Z.P. Huo, S.Y. Dai, K.J. Wang, F.T. Kong, C.N. Zhang, X. Pan, X.Q. Fang, Sol. Energy Mater. Sol. Cells 91 (2007) 1959–1965.
[21] P. Wang, S.M. Zakeeruddin, P. Comte, I. Exnar, M. Grätzel, J. Am. Chem. Soc. 125 (2003) 1166–1167.
[22] K. Lee, P. Chen, C. Lee, K. Ho, J. Power Sources 190 (2009) 573–577.
[23] H. Yang, C.Z. Yu, Q.L. Song, Y.Y. Xia, F.Y. Li, Z.G. Chen, X.H. Li, T. Yi, C.H. Huang, Chem. Mater. 18 (2006) 5173–5177.
[24] N. Mohmeyer, P. Wang, H.-W. Schmidt, S.M. Zakeeruddin, M. Grätzel, J. Mater. Chem. 14 (2004) 1905–1909.
[25] N. Mohmeyer, D.B. Kuang, P. Wang, H.-W. Schmidt, S.M. Zakeeruddin, M. Grätzel, J. Mater. Chem. 16 (2006) 2978–2983.
[26] G.D. Rees, B.H. Robinson, Adv. Mater. 5 (1993) 608–619.

[27] G. Haering, P.L. Luisi, J. Phys. Chem. 90 (1986) 5892–5895.
[28] R.J. Phillips, W.M. Deen, F.J. Brady, J. Colloid Interface Sci. 139 (1990) 363–373.
[29] R.J.H. Hafkamp, P.A. Kokke, H.P.M. Geurts, A.E. Rowan, M.C. Feiters, R.J.M. Nolte, I.M. Danke, Chem. Commun. (1997) 545–546.
[30] T. Schamper, M. Jablon, M.H. Randhawa, A. Senatore, J.D. Warren, J. Soc. Cosmet. Chem. 37 (1986) 225–231.
[31] U. Beginn, B. Tartsch, Chem. Commun. (2001) 1924–1925.
[32] P. Terech, R.G. Weiss, Chem. Rev. 97 (1997) 3133–3159.
[33] L.H. Hu, S.Y. Dai, J. Weng, S.F. Xiao, Y.F. Sui, Y. Huang, S.H. Chen, F.T. Kong, X. Pan, L.Y. Liang, K.J. Wang, J. Phys. Chem. B 111 (2007) 358–362.
[34] C.W. Shi, S.Y. Dai, K.J. Wang, X. Pan, L.Y. Zeng, L.H. Hu, F.T. Kong, L. Guo, Electrochim. Acta 50 (2005) 2597–2602.
[35] C.N. Zhang, J. Dai, Z.P. Huo, X. Pan, L.H. Hu, F.T. Kong, Y. Huang, Y.F. Sui, X.Q. Fang, K.J. Wang, S.Y. Dai, Electrochim. Acta 53 (2008) 5503–5508.
[36] B.M. Quinn, Z. Ding, R. Moulton, A.J. Bard, Langmuir 18 (2002) 1734–1742.
[37] Z.P. Huo, S.Y. Dai, C.N. Zhang, F.T. Kong, X.Q. Fang, L. Guo, W.Q. Liu, L.H. Hu, X. Pan, K.J. Wang, J. Phys. Chem. B 112 (2008) 12927–12933.
[38] J.N. Soderberg, A.C. Co, A.H.C. Sirk, V.I. Birss, J. Phys. Chem. B 110 (2006) 10401–10410.
[39] O.A. Petrii, R.R. Nazmutdinov, M.D. Bronshtein, G.A. Tsirlina, Electrochim. Acta 52 (2007) 3493–3504.
[40] J. Bisquert, J. Phys. Chem. B 106 (2002) 325–333.
[41] Q. Wang, J. Moser, M. Grätzel, J. Phys. Chem. B 109 (2005) 14945–14953.
[42] B.A. Gregg, F. Pichot, S. Ferrere, C.L. Fields, J. Phys. Chem. B 105 (2001) 1422–1429.
[43] A. Hagfeldt, M. Grätzel, Chem. Rev. 95 (1995) 49–68.
[44] R. Komiya, L.Y. Han, R. Yamanaka, A. Islam, T. Mitate, J. Photochem. Photobiol. A: Chem. 164 (2004) 123–127.